

Controlled Vortex Formation and Facilitated Energy Transfer within Aggregates of Colloidal CdS Nanorods

Whi Dong Kim,[†] Weon-Sik Chae,^{*,‡} Wan Ki Bae,^{*,§} and Doh C. Lee^{*,†}

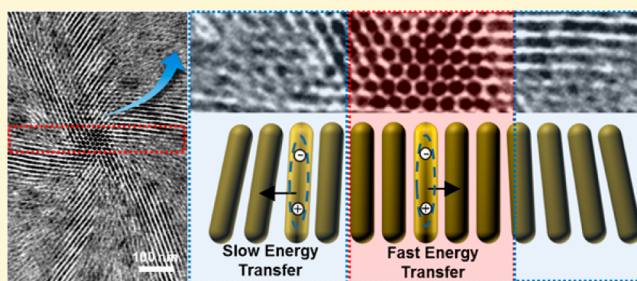
[†]Department of Chemical and Biomolecular Engineering (BK21+ Program), KAIST Institute for the Nanocentury, Korea Advanced Institute of Science and Technology (KAIST), Daejeon 305-701, Korea

[‡]Korea Basic Science Institute, Daegu 702-701, Korea

[§]Photo-Electronic Hybrids Research Center, Korea Institute of Science and Technology (KIST), 14-gil 5, Hwarang ro, Seongbuk-gu, Seoul 136-791, Korea

Supporting Information

ABSTRACT: Vortex formation is observed in transmission electron microscopy (TEM) images of colloidal CdS nanorod (NR) aggregates. Upon adding polar (poor) solvents into the NR dispersion, the NRs passivated with alkylphosphonic acids start flocculating. When NR clusters are deposited on a TEM grid, the tips of the NRs are immobilized on the substrate, and capillary forces give rise to a net inward tilting as the solvent evaporates, eventually leading to the formation of vortices. Solvent polarity turns out to play a critical role in controlling the structure of vortices. Fluorescence lifetime imaging microscopy (FLIM) of the ensembles reveals that the vortex structures have profound influence on the energy transfer rate within the NR assembly.



INTRODUCTION

The elongated geometry in semiconductor nanorods (NRs) gives rise to unique optical properties, such as linearly polarized emission¹ and the Stark effect.² Being able to assemble NRs into controlled geometries would allow best use of such properties, bring forth additional physical properties, and harness their use in a variety of applications.^{3–5} Colloidal synthesis proved to be versatile in achieving geometric and crystallographic uniformity of NRs desired for assembly.⁶ Monodisperse NRs can self-assemble into periodically ordered clusters, which is one of the most studied tools to achieve defect-free arrangements of nanomaterials.^{7–9}

Self-assembly of colloidal NRs is typically driven by fine-tuning inter-NR forces that bring the NRs together. By and large, there are two approaches: assembly of NRs on a substrate with solvent drying^{7,10,11} and assembly of NRs within solution or at the liquid interface.^{8,9,12,13} The former usually capitalizes on the increase of capillary forces between neighboring NRs when the solvent evaporates.^{14,15} Similarly, but with more control, NRs can assemble in a liquid dispersion when their solubility diminishes. Hydrophobic attraction, van der Waals force, and dipole–dipole interactions can account for in-solution aggregation.¹⁶ Yet, even very small perturbations during assembly result in defects, hampering the formation of long-range periodicity. Notably, some of the “successful” assemblies exhibited mesmerizing vortex structures. A vortex is observed when rod-shaped objects tilt within assembled clusters in a way that the obliqueness forms a line defect rotationally diverging from the center. For instance, Figure 3 of

ref 7, Figure 9 of ref 17, Figure 3 of ref 18, and Figure 4 of ref 19 showed vortices in assembled colloidal NRs; however, the control or mechanism of vortex formation in NR clusters was largely underexplored, and thorough discussion was lacking, likely due to the difficulty in controlling the vortex structures.

Here, we report controlled self-assembly of colloidal CdS NRs into vortex structures. Interaction forces acting between NRs and between NRs and substrates are estimated in a simplified model, whose predictability is tested and discussed in line with in-solution X-ray scattering results. In addition, the relationship between the structure of NR assemblies and their optical characteristics is investigated.

EXPERIMENTAL SECTION

Chemicals. Cadmium oxide (CdO, ≥99.99%, trace metals basis), trioctylphosphine oxide (TOPO, 99%), trioctylphosphine (TOP, 97%), sulfur (S, 97%), nonanoic acid (≥97%), and dimethyl sulfoxide (DMSO, ≥99.5%) were purchased from Sigma-Aldrich. Octadecylphosphonic acid (ODPA, ≥98%) was purchased from TCI.

Preparation of CdS NRs. We synthesized CdS NRs using a previously reported recipe by Robinson et al. with minor modification.²⁰ A total of 210 mg of CdO, 2.75 g of TOPO, and 1.06 g of ODPA were mixed in a three-neck flask and heated to 120 °C under a vacuum for 1 h. After that, we heated the

Received: November 21, 2014

Revised: March 31, 2015

Published: April 2, 2015

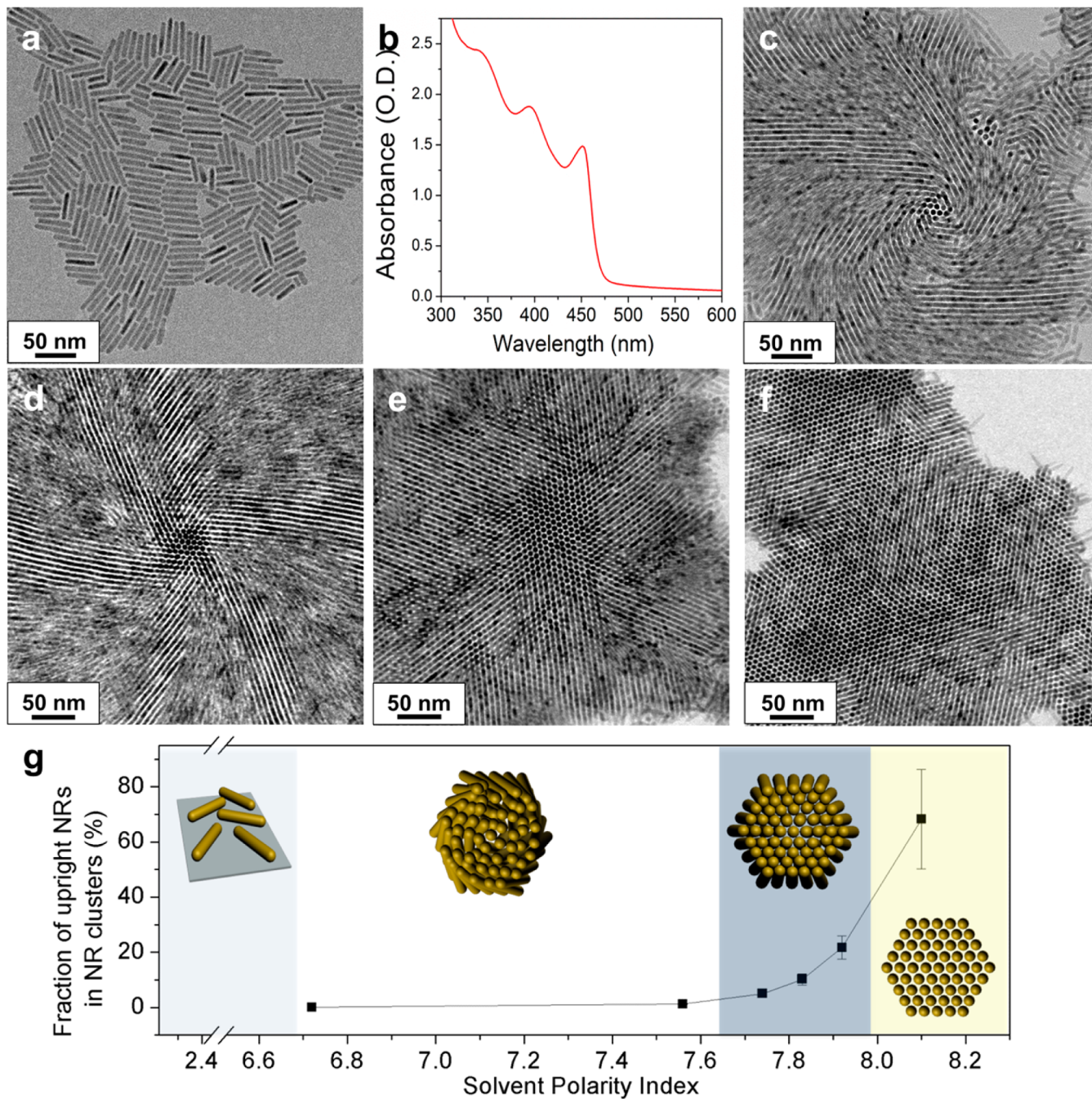


Figure 1. (a) TEM image and (b) absorption spectrum of CdS NRs. (c–f) TEM image of CdS NRs assembled by injecting 0.05 mL of toluene stock solution containing CdS NRs into 2 mL of various cosolvent mixtures ((c) toluene/DMSO = 1:10 ($P' = 6.72$), DMSO/water = (d) 80:20 ($P' = 7.56$), (e) 65:35 ($P' = 7.83$), (f) 50:50 ($P' = 8.10$)) and depositing onto a carbon-coated grid. (g) Solvent polarity-dependent fraction of upright NRs in the NR cluster. Inset diagrams illustrate representative formations at each polarity index.

solution to 320 °C for 30 min under Ar flow, which was cooled to 120 °C under a vacuum for 30 min. Then, the temperature was raised back to 320 °C under Ar flow, at which 1.5 g of TOP was added, followed by dropwise injection of TOP-S precursor (prepared by dissolving 1.38 g of TOP and 0.12 g of S in a drybox at 70 °C for 3 h). Ten minutes after injection completion, the solution was cooled to room temperature for termination of reaction, and 10 mL of toluene was added. The resulting dispersion was centrifuged at 4000 rpm for 10 min. The centrifugation resulted in precipitation, which was collected and redispersed in 7 mL of toluene and 2 mL of nonanoic acid. Then, 15 mL of hexane and 15 mL of methanol

were slowly added, followed by centrifugation at 4000 rpm for 10 min. The hexane–methanol washing step was repeated two more times. The final stock solution is prepared by dispersing in toluene with adjusted concentration (10 mg/mL).

Aggregation of CdS NRs. In order to flocculate CdS NRs in solution, 50 μL of stock solution was added to 2 mL of polar solvent mixture, and then the solution was immediately sonicated for approximately 30 s. After 1 h, the assemblies were deposited by drop-casting onto carbon- (FCF-200-Cu, Electron Microscopy Sciences) or silica-coated (SF200-Cu, Electron Microscopy Sciences) copper grids and then were dried at 80 °C.

Characterization. The colloidal NRs and formation of assembly were examined using transmission electron microscopy (TEM, Tecnai F20 (200 kV), FEI company). Absorption spectra were recorded using a UV-vis spectrometer (UV3600, Shimadzu). To investigate the structural formation of aggregated NRs in solution, small-angle X-ray scattering (SAXS, D/MAX-2500, Rigaku Corporation) measurements were carried out. For a measurement, CdS NRs clusters in a solution were sealed in a quartz capillary tube ($\phi = 1$ mm, GLAS Technik). The scattered signal was collected with a charge coupled device (CCD) area detector. Corrected scattering patterns were transformed into a function of scattering vector q ($q = 4\pi \sin(\theta)/\lambda$), where θ is half of the scattering angle and λ is the wavelength of X-ray radiation (1.24 Å). The areal fraction of upright NRs in each sample was obtained by dividing the area of upright NRs in the NR cluster with the overall area of the NR cluster using the ImageJ software. More than 10 NR clusters were counted for each sample.

Time-Resolved Photoluminescence (TRPL) Imaging. We conducted TRPL imaging of assembled CdS NRs using an inverted-type scanning confocal microscope (Picoquant MicroTime-200) with a 100× oil-immersion objective. An excitation source is a 375 nm single-mode pulsed diode laser with a pulse width of 240 ps and a 10 MHz repetition rate, and an average power of <1 μW. Emissions from the assembled NRs were collected with a dichroic mirror (AHF Z375RDC), a long-pass filter (AHF HQ405lp), a 50 μm pinhole, and a single-photon avalanche diode (SPAD) after passing the neutral density filter, in which the photon counting rate was maintained around 1% of the excitation rate. Data acquisition was based on a time-correlated single photon counting technique. Measured TRPL images were presented in fast TRPL imaging mode provided by the SymPhoTime operating software (ver. 5.1.3). The TRPL images typically present a longer average lifetime than the average ($1/e$) PL lifetime measured from PL spectroscopy. For each solvent condition, we estimated average lifetime from TRPL images by measuring five or more NR clusters. To investigate energy transfer (ET) between NRs in the NR aggregates, the PL signal from the NR samples was filtered in three wavelength ranges: (i) 405–800 nm, (ii) 480 ± 10 nm, and (iii) 650 ± 10 nm. The three emission ranges represent overall, band-edge, and surface trap emissions of NRs, respectively. Figure S1 shows a resulting TRPL image that reflects the three emission ranges.

■ RESULTS AND DISCUSSION

As shown in Figure 1a, colloidal CdS NRs were prepared with relatively narrow size dispersion: 5.8 ± 0.3 nm ($\sigma = 5.2\%$) in diameter and 41.2 ± 5.2 nm ($\sigma = 12.6\%$) in length. An absorbance spectrum shows a distinct 1S band-edge transition peak at 450 nm, which validates the size uniformity of prepared CdS NRs (Figure 1b). Into the well-defined CdS NR solutions (10 mg/mL in toluene), we introduced polar cosolvents consisting of different concentrations of dimethyl sulfoxide (DMSO) and water. The change in solvent polarity induced flocculation of CdS NRs in solution, as observed in the change of turbidity in the mixed solutions (Figure S2). We note that the dispersion is colloidally stable for a day under lab conditions, enabling us to perform reproducible experiments.

TEM analysis reveals that CdS NRs aggregated in the turbid solution into isolated clusters of 0.5–1 μm size (Figure 2). Strikingly, NR arrangement within the clusters appears to

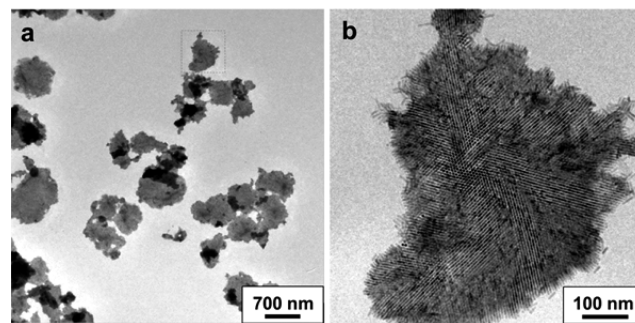


Figure 2. (a) Low-resolution TEM image of CdS NR clusters and (b) high-resolution TEM image of the rectangle marked in (a).

change as solvent polarity varies (Figure 1c–f). As the solvent becomes more polar, a center domain of upright NRs grows larger (Figure 1g). The fraction of upright NRs in NR clusters was calculated using the ImageJ software: the area of upright NRs in a NR cluster was divided by overall area of the cluster. The average was obtained after running the calculation for at least 10 different clusters under each polarity condition (Table S1). At DMSO/water/toluene = 1:1:0.05 (volume ratio, polarity index $P' = 8.10$), some clusters exhibit upright NRs extending into the entire island domain. To the best of our knowledge, this is the first observation that the degree of vortex formation can be controlled by systematic variation of an experimental parameter. Modulating the interactions between neighboring NRs is the key to controlled aggregation and vortex formation of NRs in solution. Obviously, changing the solvent polarity is one easy way to regulate the interactions between NRs, as solvent polarity is directly relevant to the relative hydrophobic attraction of neighboring NRs.

We speculate that the spacing between NRs in the NR dispersion plays a critical role in vortex formation during solvent evaporation. To understand the mechanism of vortex formation, we investigated CdS NR flocculation upon the addition of polar (poor) solvents into the NR dispersion. Small-angle X-ray scattering (SAXS) spectra reveal that NRs flocculate into 2D hexagonal closed packed cylinders (Figure 3a).²¹ (Here, q_1 , q_2 , q_3 , and q_4 reveal the ratio $q_x/q_0 = \sqrt{1}$, $\sqrt{3}$, $\sqrt{4}$, and $\sqrt{9}$, respectively, indicating the formation of hexagonal close packed NRs; q_1 , q_2 , q_3 , and q_4 denote (100), (110), (200), and (300) planes of hexagonal structure, respectively;²² q^* corresponds to the ligand bilayer.²³) At low q , the intensity of scattering reveals a power-law decay between q^{-2} and q^{-3} (Figure S5). The increase of intensity at low q is indicative of a change in total scattering volume. This exponential decay is ascribed to aggregation of NRs in solution.^{24,25} The q^1 and q^* peaks shift as the solvent polarity increases, which indicates that the center-to-center and side-to-side distances between NR flocs, respectively, decrease as the solvent polarity increases (Table 1). We attribute the gradual decrease in the interparticle spacing in NR flocs upon the addition of polar solvent to (i) the repulsive forces between NRs and the medium and (ii) the shrinkage of the hydrodynamic volume of surface capping ligands, octadecyl-phosphonic acid (ODPA) in our case.²⁶

In all of the cases we analyzed from TEM images, the average inter-NR spacing was identical (~1.1 nm) regardless of vortex structures. This is in contrast to SAXS results, in which polar solvents reduced the spacing. We believe that the hydrophobic interactions and ligand swelling, which account for the spacing

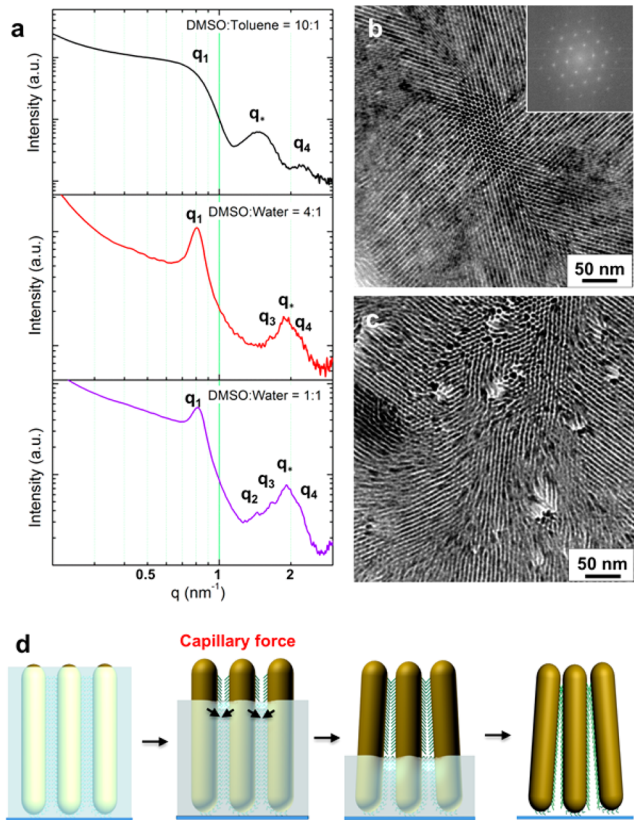


Figure 3. (a) SAXS data of CdS NRs assembled with varying solvent polarity. (b,c) TEM images of assembled CdS NRs in cosolvent mixture (DMSO/water = 65:35) deposited onto (b) carbon- and (c) silica-coated grids. Inset of b is a fast Fourier-transform image, which represents 6-fold symmetry of assembly formation. (d) Schematic illustration of NR tilting during solvent evaporation, with acting forces between NRs and NRs and substrates.

Table 1. Center-to-Center Distances and Edge-to-Edge Separations Measured Using SAXS and TEM for CdS NRs Dispersed in Different Solvents

solvent (polarity index)	measurement	D_{ss} (nm) a (q (nm $^{-1}$))	D_{cc} (nm) b (q (nm $^{-1}$))
DMSO/toluene 10:1 (6.72)	SAXS	9.17 (0.72)	4.23 (1.49)
DMSO/water 4:1 (7.56)	TEM	6.8	1
DMSO/water 1:1 (8.1)	SAXS	7.64 (0.81)	3.39 (1.88)
	TEM	6.8	1.1
	SAXS	7.55 (0.82)	3.33 (1.91)
	TEM	6.9	1.1

^aSide-to-side spacing between NRs. ^bCenter-to-center distance between NRs.

variations, did not come into play after solvent evaporation.²⁷ NR-to-NR distance reduces to an equilibrium value of 1.1 nm, which corresponds to the length of interdigitated ODPA.²⁸ While comprehensive analysis on the physical nature of the interactions is yet unavailable, we postulate that the spacing between NRs within flocculated NR clusters allows the NRs to tilt during solvent evaporation and eventually determines the degree of vortex formation.

To examine the influence of NR-substrate binding on the vortex formation, we used a silica-coated TEM grid whose surface is hydrophilic. Figure 3b and c show representative

TEM images of NR clusters collected on carbon-coated (water contact angle $\geq 75^\circ$) and silica-coated (water contact angle $= \sim 15^\circ$) TEM grids, respectively. The use of a silica-coated TEM grid results in rather random tilting, while a carbon-coated grid seems to trigger 6-fold symmetry in the tilting due to the hexagonal faceting of the sides of the wurtzite CdS NRs combined with crystallographic registry between NRs in the array.²⁹ NRs immobilized by adhesion to the carbon substrate make this unique vortex formation (see Figure 3d).

The vortex structures observed in the present study are structurally similar to disclinations, a type of defect resulting from the tilting of one-dimensional molecular liquid crystals. Various external forces were found to be responsible for the formation of disclinations.³⁰ In our case, NRs undergo dynamic assembly and aggregate into a quasi-equilibrium hexagonal structure in solution, as indicated by the sharp characteristic peaks in in-solution SAXS data. Capillary forces become the external force that disrupts the equilibrium of the NR aggregation during solvent evaporation, as illustrated in Figure 3d. When the solvents evaporate, the capillary attraction between the NRs effectively pulls them inward. Such capillary-induced deformation was reported in a previous study on polymer micropillars, which formed helical structures when capillary force induced the tilting and bending while one side of the polymer rods were fixed on a substrate.³¹ The evaporation of solvent gives rise to capillary forces in NR clusters. As one side of the NRs is bound to a carbon-coated TEM grid, the tilting of hexagonally packed NRs results in the 6-fold vortex-like structure. On the other hand, on a silica-coated TEM grid, a weak adhesion between NRs and the grid permits sliding of NRs and hence irregular tilting during the solvent evaporation. Therefore, the geometric structure of preassembled NR cluster, interaction with substrate, and the inter-NR spacing play critical roles for varying degree of vortex formation. Preassembled NR clusters with larger interparticle spacing undergo much dramatic volume contraction, and transform into vortex structures with lower upright NR areal fraction and higher NR tilting angle (Figure 1c–f).

As NRs form tilted, vortex-rich clusters, the ensemble would exhibit optical properties uniquely reflecting NR-to-NR interactions. We performed FLIM analysis on (i) NR solution in toluene, (ii) NRs with long-range vertical alignment (e.g., Figure 1e), (iii) NRs with random tilting (e.g., Figure 3c), and (iv) NRs with vortex structure (e.g., Figure 1d) on a substrate. Figure 4a–c shows microscopy images with samples ii–iv with a color index of FL in each pixel area. In all of the FLIM images, the size of each isolated emitting area is around 0.5–1 μm , which is in good agreement with the size of NR clusters measured from TEM images. In Figure 4d, FL decay curves of the ensembles of samples i–iv are plotted. We estimated FL decay primarily using average lifetime, in which fluorescent intensity becomes $1/e$ of the initial intensity.³² The average FLs and FLIM images of assembled NRs exhibit a surprising, yet coherent, difference depending on the arrangement of NRs in the clusters. As shown in Figure 4d, vertically arranged NRs show the shortest average FL (0.31 ns). The FLIM image in Figure 4a corroborates the rapid and uniform FL decay throughout the whole island. In the case of vortex structures, the average FL is slightly longer (0.39 ns). It is noteworthy that Figure 4c demonstrates inhomogeneous spatial distribution of FL decay: faster at the center and slower at the edge. Ensemble FL decay in the irregular NR film is similar to the case of vortex

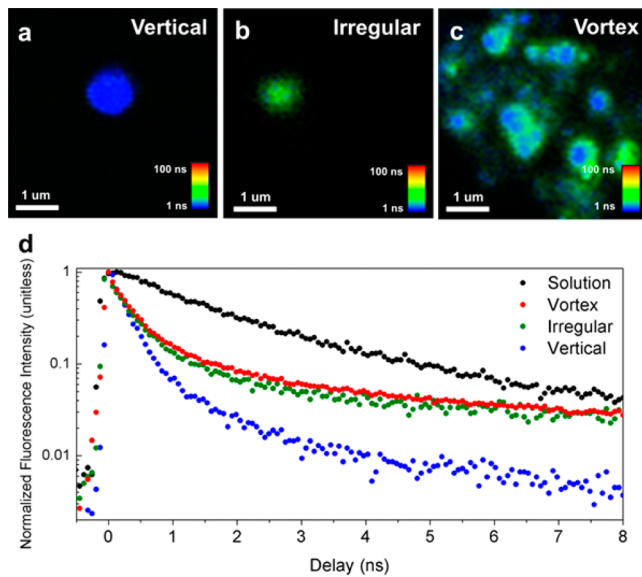


Figure 4. FLIM images at a 480 ± 10 nm wavelength of (a) vertical, (b) irregular, (c) vortex NR formations, with fluorescence-lifetime (FL) represented by gradient color bar. (d) Ensemble FL decay curves of NRs assembled in varying structures.

islands. However, as shown in Figure 4b, homogeneous color in irregular clusters is a clear-cut difference.

To elucidate FL alteration with varying structures, we consider the resonance energy transfer (ET) in the assembled NRs.³³ ET between CdS NRs is known to occur in assembled NRs and, in our case, is believed to reduce the average FL by “opening” a new nonradiative recombination pathway in contrast to NRs in solution.

Including the ET term in FL, the recombination rate can be expressed as the following:

$$k_{\text{total}} = k_r + k_{\text{intra-nr}} + k_{\text{ET}} \quad (1)$$

where

k_{total} = total recombination rate

k_r = radiative recombination rate

$k_{\text{intra-nr}}$ = intrapartical non – radiative recombination rate

k_{ET} = energy transfer rate

From eq 1, we can estimate k_{ET} , based on the assumption that k_r and $k_{\text{intra-nr}}$ of NRs remain unchanged after assembly. We validated the assumption by redispersing CdS NRs that flocculated upon the addition of polar solvents into hexane and measuring fluorescence quantum yield of the sample. It turns out that the quantum yield did not alter during the assembly process, which indicates that nonradiative intra-NR recombination remain nearly the same. The ET rate was estimated to be 2.63, 1.96, and 2.22 ns⁻¹ in the vertical, vortex, and irregular assembly, respectively. In general, ET rate is given by

$$K_T(r) = \frac{Q_D K^2}{\tau_D r^6} \left(\frac{9000(\ln 10)}{128\pi^5 N n^4} \right) \int_0^D F_D(\lambda) \epsilon_A(\lambda) \lambda^4 d\lambda \quad (2)$$

where Q_D is the quantum yield of the donor in the absence of an acceptor, n is the refractive index of the medium, N is

Avogadro’s number, r is the distance between a donor and an acceptor, τ_D is the lifetime of the donor in the absence of an acceptor, $\epsilon_A(\lambda)$ is the extinction coefficient of the acceptor at λ , and the term of K^2 is a factor describing the relative orientation of the transition dipoles of the donor and acceptor. Considering NR dimensions and factoring fixed variables into α , eq 2 can be expressed as

$$K_T(r) = \alpha \frac{\kappa^2}{r^3} \quad (3)$$

In the vertical assembly, the average distance between NRs is ~ 1.1 nm and the orientation factor is 1.³⁴ In the case of vortex structures, the average distance between NRs was analyzed from TEM images (see Figure S5 and Supporting Information for detailed calculation). From the analysis, we obtained $r = 1.21 \pm 0.02$ nm and $\kappa^2 = 0.9998$ in randomly chosen vortex structures. The estimation led us to conclude that increased inter-NR distance is responsible for the reduced ET rate in the vortex-including clusters. On the other hand, change in the orientation factor (by 0.02%) hardly accounts for the change in ET rate in the vortex structure. Using eq 3, we compared the ET rates in NRs of vertical arrays and of vortex structures. The calculation yields that the ET rate in vortex clusters is 0.74 of that in aligned NRs. The ET rate change estimated from the FL decay curve is in striking agreement with the calculation: $k_{\text{ET(vortex)}}/k_{\text{ET(vertical)}} = 0.75$ (Table 2). In the case of random

Table 2. FL and Energy Transfer Rate of Colloidal and Assembled CdS NRs

sample	QY (%)	τ_0^a (ns)	τ_{ET}^b (ns)	k_{ET}^c (ns ⁻¹)
toluene solution	9.8	1.64		
film/vertical array		0.31 ± 0.036	0.38	2.63
film/irregular array		0.35 ± 0.025	0.45	2.22
film/vortex structure		0.39 ± 0.037	0.51	1.96

^aAverage (1/e) FL. ^bCharacteristic energy transfer time. ^cEnergy transfer rate.

NRs, it is difficult to calculate the ET rate using eq 2 or 3, because of the difficulty in measuring the distance between NRs. One would surmise that the random array gives rise to a longer distance between NRs compared to the vertical array and thus has slower ET. From the ET study, we can explain the inhomogeneous spatial distribution of FL decay in vortex clusters. At the eye of vortex structures, hexagonally packed, upright NRs, practically the same arrangement as vertical arrays, form a center domain, whose size is several hundred nanometers as measured in both TEM and FLIM images. On the other hand, tilted NRs located at the edge show relatively slow ET as the effective NR-to-NR distance increases because of the obliqueness. Therefore, spatial variation of FL lifetime in one NR cluster results from the uniqueness of vortex structures, in which hexagonally packed and tilted NRs coexist. In addition, in the case of trap emission from NR cluster with vortex structure, ET does not occur because of the lack of absorption–emission overlap in the range of trap emission. Consequently, homogeneous distribution of FL decay of trap emission corroborates that ET was the main reason for lifetime variance shown in Figure S1c.

In summary, colloidal CdS NRs assemble with controllable vortex structures. SAXS analysis reveals that the change in inter-NR distance within NR clusters in suspension directly relates to the solvent polarity, as more polar solvents induce more

densely packed in-solution clustering. Subsequent solvent evaporation during TEM sample preparation gives rise to capillary forces, which effectively pull the NRs together and cause tilting, with the bottom of the NRs anchored on the TEM grid. The spacing between NRs in a NR cluster becomes a determining factor in the degree of vortex formation. FLIM analysis and ensemble FL decay studies demonstrate that ET kinetics is significantly altered when vortex structures evolve.

■ ASSOCIATED CONTENT

Supporting Information

Details about synthesis, characterization and additional results (TEM and photograph images and FLIM). This material is available free of charge via the Internet at <http://pubs.acs.org>.

■ AUTHOR INFORMATION

Corresponding Authors

*E-mail: wschae@kbsi.re.kr.

*E-mail: wkbae@kist.re.kr.

*E-mail: dclee@kaist.edu.

Author Contributions

The manuscript was written through contributions of all authors. All authors have given approval to the final version of the manuscript.

Notes

The authors declare no competing financial interests.

■ ACKNOWLEDGMENTS

This work was supported by the New & Renewable Energy Core Technology Program of the Korea Institute of Energy Technology Evaluation and Planning (KETEP) in the Ministry of Trade, Industry & Energy, Republic of Korea (No. 20133030011330 and No. 20133010011750), and by the National Research Foundation (NRF) grant funded by the Korean government (grants NRF-2011-0030256 and NRF-2014R1A2A2A01006739). This work was also in part supported by KIST internal funding (2E25393).

■ REFERENCES

- (1) Hu, J. T.; Li, L. S.; Yang, W. D.; Manna, L.; Wang, L. W.; Alivisatos, A. P. *Science* **2001**, *292*, 2060.
- (2) Hewa-Kasakarage, N. N.; Kirsanova, M.; Nemchinov, A.; Schmall, N.; El-Khoury, P. Z.; Tarnovsky, A. N.; Zamkov, M. *J. Am. Chem. Soc.* **2009**, *131*, 1328.
- (3) Hikmet, R. A. M.; Chin, P. T. K.; Talapin, D. V.; Weller, H. *Adv. Mater.* **2005**, *17*, 1436.
- (4) Sitt, A.; Hadar, I.; Banin, U. *Nano Today* **2013**, *8*, 494.
- (5) Xie, Y.; Liang, Y. J.; Chen, D. X.; Wu, X. C.; Dai, L. R.; Liu, Q. *Nanoscale* **2014**, *6*, 3064.
- (6) Krahne, H.; Manna, L.; Morello, G.; Figuerola, A.; George, C.; Deka, S. *Physical Properties of Nanorods*; Springer: Berlin, 2013.
- (7) Singh, A.; Gunning, R. D.; Ahmed, S.; Barrett, C. A.; English, N. J.; Garate, J. A.; Ryan, K. M. *J. Mater. Chem.* **2012**, *22*, 1562.
- (8) Baranov, D.; Fiore, A.; van Huis, M.; Giannini, C.; Falqui, A.; Lafont, U.; Zandbergen, H.; Zanella, M.; Cingolani, R.; Manna, L. *Nano Lett.* **2010**, *10*, 743.
- (9) Talapin, D. V.; Shevchenko, E. V.; Murray, C. B.; Kornowski, A.; Forster, S.; Weller, H. *J. Am. Chem. Soc.* **2004**, *126*, 12984.
- (10) Baker, J. L.; Widmer-Cooper, A.; Toney, M. F.; Geissler, P. L.; Alivisatos, A. P. *Nano Lett.* **2010**, *10*, 195.
- (11) Hung, A. M.; Konopliv, N. A.; Cha, J. N. *Langmuir* **2011**, *27*, 12322.
- (12) Zanella, M.; Bertoni, G.; Franchini, I. R.; Brescia, R.; Baranov, D.; Manna, L. *Chem. Commun.* **2011**, *47*, 203.

- (13) Zhao, N.; Liu, K.; Greener, J.; Nie, Z. H.; Kumacheva, E. *Nano Lett.* **2009**, *9*, 3077.
- (14) Yang, P. D.; Kim, F. *ChemPhysChem* **2002**, *3*, 503.
- (15) Zhang, S. Y.; Regulacio, M. D.; Han, M. Y. *Chem. Soc. Rev.* **2014**, *43*, 2301.
- (16) Sanchez-Iglesias, A.; Grzelczak, M.; Altantzis, T.; Goris, B.; Perez-Juste, J.; Bals, S.; Van Tendeloo, G.; Donaldson, S. H.; Chmelka, B. F.; Israelachvili, J. N.; Liz-Marzan, L. M. *ACS Nano* **2012**, *6*, 11059.
- (17) Sau, T. K.; Murphy, C. J. *Langmuir* **2005**, *21*, 2923.
- (18) Li, L. S.; Alivisatos, A. P. *Adv. Mater.* **2003**, *15*, 408.
- (19) Yang, P. D.; Kim, F. *ChemPhysChem* **2002**, *3*, 503.
- (20) Robinson, R. D.; Sadtler, B.; Demchenko, D. O.; Erdonmez, C. K.; Wang, L. W.; Alivisatos, A. P. *Science* **2007**, *317*, 355.
- (21) A detailed explanation on SAXS results is provided in the Supporting Information.
- (22) Petukhova, A.; Greener, J.; Liu, K.; Nykypanchuk, D.; Nicolay, R.; Matyjaszewski, K.; Kumacheva, E. *Small* **2012**, *8*, 731.
- (23) Schliehe, C.; Juarez, B. H.; Pelletier, M.; Jander, S.; Greshnykh, D.; Nagel, M.; Meyer, A.; Foerster, S.; Kornowski, A.; Klinke, C.; Weller, H. *Science* **2010**, *329*, 550.
- (24) Ustarroz, J.; Altantzis, T.; Hammons, J. A.; Hubin, A.; Bals, S.; Terryn, H. *Chem. Mater.* **2014**, *26*, 2396.
- (25) Martin, J. E.; Hurd, A. J. *J. Appl. Crystallogr.* **1987**, *20*, 61.
- (26) Leekumjorn, S.; Gullapalli, S.; Wong, M. S. *J. Phys. Chem. B* **2012**, *116*, 13063.
- (27) Zhang, J.; Luo, Z. P.; Martens, B.; Quan, Z. W.; Kumbhar, A.; Porter, N.; Wang, Y. X.; Smilgies, D. M.; Fang, J. Y. *J. Am. Chem. Soc.* **2012**, *134*, 14043.
- (28) Li, M.; Schnablegger, H.; Mann, S. *Nature* **1999**, *402*, 393.
- (29) Ahmed, S.; Ryan, K. M. *Nano Lett.* **2007**, *7*, 2480.
- (30) Li, L. S.; Walda, J.; Manna, L.; Alivisatos, A. P. *Nano Lett.* **2002**, *2*, 557.
- (31) Pokroy, B.; Kang, S. H.; Mahadevan, L.; Aizenberg, J. *Science* **2009**, *323*, 237.
- (32) Taguchi, S.; Saruyama, M.; Teranishi, T.; Kanemitsu, Y. *Phys. Rev. B* **2011**, *83*, No. 155324.
- (33) Chin, P. T. K.; Hikmet, R. A. M.; Meskers, S. C. J.; Janssen, R. A. *J. Adv. Funct. Mater.* **2007**, *17*, 3829.
- (34) Lakowicz, J. R. *Principle of Fluorescence Spectroscopy*, 3rd ed.; Springer: New York, 2006; p 448.